

This discussion paper is/has been under review for the journal Atmospheric Chemistry and Physics (ACP). Please refer to the corresponding final paper in ACP if available.

# Mixing layer height and the implications for air pollution over Beijing, China

G. Tang<sup>1</sup>, J. Zhang<sup>2</sup>, C. Münkel<sup>3</sup>, T. Song<sup>1</sup>, B. Hu<sup>1</sup>, K. Schäfer<sup>4</sup>, Z. Liu<sup>1</sup>, J. Xin<sup>1</sup>, P. Suppan<sup>4</sup>, and Y. Wang<sup>1</sup>

<sup>1</sup>State Key Laboratory of Atmospheric Boundary Layer Physics and Atmospheric Chemistry (LAPC), Institute of Atmospheric Physics, Chinese Academy of Sciences, Beijing 100029, China

<sup>2</sup>Key Laboratory of Middle Atmosphere and Global Environment Observation (LAGEO), Institute of Atmospheric Physics, Chinese Academy of Sciences, Beijing 100029, China

<sup>3</sup>Vaisala GmbH, 22607 Hamburg, Germany

<sup>4</sup>Karlsruhe Institute of Technology (KIT), Institute of Meteorology and Climate Research, Atmospheric Environmental Research (IMK-IFU), 82467 Garmisch-Partenkirchen, Germany

Received: 3 September 2015 – Accepted: 1 October 2015 – Published: 21 October 2015

Correspondence to: Y. Wang (wys@mail.iap.ac.cn)

Published by Copernicus Publications on behalf of the European Geosciences Union.

ACPD

15, 28249–28288, 2015

Mixing layer height  
and air pollution over  
Beijing

G. Tang et al.

Title Page

Abstract

Introduction

Conclusions

References

Tables

Figures

◀

▶

◀

▶

Back

Close

Full Screen / Esc

Printer-friendly Version

Interactive Discussion



## Abstract

The mixing layer is an important meteorological factor that affects atmospheric pollution. A study of atmospheric pollution in the Beijing area was performed from July 2009 to December 2012, using a ceilometer, to observe and study the atmospheric mixing layer height (MLH). Based on a comparison and validation of multiple types of data, we evaluated the quality of the MLH data as observed by the ceilometer and found that the ceilometer underestimates MLH during neutral stratification caused by strong winds, whereas it overestimates MLH during dust crossing. By combining conventional meteorological data and PM<sub>2.5</sub> and PM<sub>10</sub> observational data, we screened the observational results for the MLH, and the ceilometer observations were fairly consistent with the meteorological radiosonde profile results. The correlation coefficient is more than 0.9, and the effective rate of acquired data is near 80 %. Further analysis of the variation in the MLH indicates that the MLH in the Beijing area exhibits the feature of being low in autumn and winter and being high in spring and summer. There is a significant correlation between the variation in the MLH and the sensible heat flux, whereas the diurnal variation in the mixing layer during summer is affected by the circulation of mountainous plain winds. By applying visibility as the index for the classification of atmospheric pollution degree, it is found that in comparison with a clear day, the variation of sensible heat and buoyancy term in turbulent kinetic energy (TKE) of a slight haze day is insignificant, but the reduction of shear term in TKE is near 70 % when visibility decreased from 10 to 5 km; in comparison with the slight haze day, the variation of shear term in TKE of medium and heavy haze days is insignificant, but the declination of sensible heat and buoyancy term in TKE are about 60 % when visibility decreased from 5 to 1 km. Although the correlation between the daily variation of MLH and visibility is very poor, the correlation between them is significantly enhanced as the relative humidity increases beyond 80 %. This characterizes the generation of humidity-related physiochemical processes as the main source of atmospheric particles under heavy pollution, whereas the dissipation of atmospheric particles mainly depends on the MLH. The pre-

## Mixing layer height and air pollution over Beijing

G. Tang et al.

[Title Page](#)

[Abstract](#)

[Introduction](#)

[Conclusions](#)

[References](#)

[Tables](#)

[Figures](#)

◀

▶

[Back](#)

[Close](#)

[Full Screen / Esc](#)

[Printer-friendly Version](#)

[Interactive Discussion](#)



sented results on the atmospheric mixing layer and its thermal dynamic structure under different degrees of pollution provide a scientific basis for improving the meteorological and atmospheric chemistry models and the forecasting and warning of atmospheric pollution.

## 5 1 Introduction

The mixing layer is formed because of discontinuous turbulence between the upper and lower layers resulting from discontinuity in temperature stratification. The height to which the atmospheric mixing layer extends is the mixing layer height (MLH). The atmospheric MLH is an important meteorological factor that affects atmospheric pollution 10 because it affects the vertical diffusion capability of atmospheric pollutants and water vapour gradients; therefore, it affects the generation and dissipation of pollutants (Stull, 1988). Continuous observations of the MLH are helpful for improving parameterization schemes of the model boundary layer and beneficial for improving the simulation accuracy of meteorological models and optimizing the simulation results for pollutants.

15 Three primary observation methods are used to determine the MLH: meteorological sounding profiles, aeroplane surveys, and ground-based remote sensing. As the most conventional observation approach, meteorological radiosonde profiles have a large number of observation stations distributed globally, and observational data quality is high. However, because the observational cost is relatively high, only two observations 20 at 00:00 and 12:00 UTC are available from most stations (Seibert et al., 2000). As solar radiation increases in the morning, the growth rate for the MLH reaches hundreds of metres to 1000 m per hour at the stage of fast convection development, and even the hourly observations of the sounding profile could not seize important observational information of MLH (Seibert et al., 2000). Although aeroplane surveys can obtain high-resolution variations of meteorological and pollutants profiles, the constraints of air traffic control, weather conditions, and observation cost reduce these data to a limited time period. Therefore, to acquire continuous observations with high spatial and temporal 25

ACPD

15, 28249–28288, 2015

## Mixing layer height and air pollution over Beijing

G. Tang et al.

<a href="#">Title Page</a>	
<a href="#">Abstract</a>	<a href="#">Introduction</a>
<a href="#">Conclusions</a>	<a href="#">References</a>
<a href="#">Tables</a>	<a href="#">Figures</a>
<a href="#">◀</a>	<a href="#">▶</a>
<a href="#">◀</a>	<a href="#">▶</a>
<a href="#">Back</a>	<a href="#">Close</a>
<a href="#">Full Screen / Esc</a>	
<a href="#">Printer-friendly Version</a>	
<a href="#">Interactive Discussion</a>	



resolution, ground-based remote sensing has become the most advanced approach for measuring the MLH.

There are three methods of performing ground-based remote sensing: acoustic radar (sodar – sound detection and ranging), laser radar (lidar – light intensity detection and ranging) and electromagnetic radar (Doppler radar). Sodar can obtain the vertical profile of wind and temperature data; thus, it can be used to further calculate the MLH. Lidar can obtain the vertical profile of variations in the aerosol concentration and discern the atmospheric MLH by calculating the height for sudden changes of aerosol profile. Doppler wind radar can obtain variations in the wind vectors at different altitudes and identify variations in the mixing layer through the wind shear. Beyrich (1997), Seibert et al. (2000), and Emeis et al. (2008) conducted three reviews of the three methods and compared their advantages and disadvantages. The sodar detection height is usually lower than 1000 m, which is not conducive for observing the MLH under convection states. Lidar observations are usually performed in the visible light band, and it could cause visual hazards when not used properly; moreover, before the application of modern laser ceilometers for this purpose, lidar observation devices are relatively costly and unlikely to become popularly used. Wind radar is easily interfered by clouds, and the observational height is limited under cloudy conditions. In recent years, lidar observational technology has developed rapidly, and an increasing number of applications have used lidar for MLH observations (White et al., 1999; Steyn, et al., 1999; Hägeli et al., 2000; Chen et al., 2001; Schneider and Eixmann, 2002; Kunz et al., 2002; Strawbridge and Snyder, 2004; He et al., 2006; Wiegner et al., 2006; Sicard et al., 2006; Hennemuth and Lammert, 2006; Emeis et al., 2007; Wang et al., 2012; Yang et al., 2013; Luo et al., 2014; Scarino et al., 2014). Furthermore, the eye-safe ceilometers CL31 and CL51 have been developed by Vaisala to observe the MLH using a near-infrared band laser. Because of the simple operation and low cost, such instruments have become the optimal solution for observing the MLH, and they have been applied to an increasing number of observations in recent years (Münkel and Räsänen, 2004; Emeis et al., 2004; Emeis and Schäfer, 2006; Eresmaa et al., 2006; Münkel et al., 2007; McKendry

**Mixing layer height and air pollution over Beijing**

G. Tang et al.

[Title Page](#)[Abstract](#)[Introduction](#)[Conclusions](#)[References](#)[Tables](#)[Figures](#)[◀](#)[▶](#)[◀](#)[▶](#)[Back](#)[Close](#)[Full Screen / Esc](#)[Printer-friendly Version](#)[Interactive Discussion](#)

et al., 2009; Kamp and McKendry, 2010; Muñoz and Undurraga, 2010; Flentje et al., 2010; Chen et al., 2011; Haeffelin et al., 2012; Emeis et al., 2012; Schween et al., 2014; Tang et al., 2015).

Beijing, located on the North China Plain, is the centre of politics, culture, and economics in China. Because of the rapid economic development, energy usage has increased, which has caused serious air pollution and frequent heavy haze days (Tang et al., 2009, 2012; Xin et al., 2010). Previous studies have indicated that visibility declines dramatically during heavy pollution periods in Beijing when the concentration of particles increases. In addition, the weather conditions generally include high humidity and low wind speed with a southerly flow, and the atmospheric stratification is stable (Ding et al., 2005; Liu et al., 2014; Zhang et al., 2015). Previous studies have provided additional descriptions of weather conditions corresponding to heavy pollution periods; however, atmospheric MLH variations are the key meteorological factors related to the occurrence, maintenance, and dissipation of heavy pollution, and they are not well understood. As for most areas in north China, the meteorological sounding data can only acquire observational data for the MLH in the morning (00:00 UTC) and at night (12:00 UTC), and observations of the convective mixing layer variations at noon are lacking. In certain studies, simulations with numerical models, short-time ground-based remote sensing, or meteorological profiles are used to provide a preliminary description of MLH variations during heavy pollution periods, but continuous high-resolution observations over a long time period have not been conducted for this region (He and Mao, 2005; Yang et al., 2005; Zhang et al., 2006; Chen et al., 2009; Quan et al., 2013; Hu et al., 2014; Zhang et al., 2015). Without acquiring the continuous high-resolution variation characteristics of the MLH through these studies, the influence of atmospheric pollution cannot be studied thoroughly (Schäfer et al., 2006).

To compensate for information gaps in the aforementioned studies, a ceilometer was used to conduct continuous high-resolution observations for 3 years and 5 months (from July of 2009 to December of 2012) in Beijing. By comparing the obtained data with multiple meteorology and pollutant data sets, we verified the applicability of the

[Title Page](#)

[Abstract](#)

[Introduction](#)

[Conclusions](#)

[References](#)

[Tables](#)

[Figures](#)

[◀](#)

[▶](#)

[◀](#)

[▶](#)

[Back](#)

[Close](#)

[Full Screen / Esc](#)

[Printer-friendly Version](#)

[Interactive Discussion](#)



ceilometer and obtained the variation characteristics of the MLH over 3 years. By combining the meteorological data, we were able to determine how variations in the mixing layer and the atmospheric diffusion capability occurred in different seasons. Finally, visibility was used to determine the degree of atmospheric pollution, and the thermal/dynamic structure inside the mixing layer was analysed under different degrees of pollution by delineating the influence of MLH variations on atmospheric pollution and revealing the critical meteorological conditions underlying the formation and dissipation of heavy atmospheric pollution in the Beijing area.

## 2 Methods

### 10 2.1 Sites and instruments

To understand the structural variations of the mixing layer in the Beijing area, we conducted observations for 3 years and 5 months (from 15 July 2009 to 31 December 2012) in Beijing. The observation sites, observation parameters, and observation time period are shown in Fig. 1 and Table 1.

15 The site used to measure the MLH was built in the tower of the Institute of Atmospheric Physics, Chinese Academy of Sciences, to the west of the Jiande bridge in the Haidian district, Beijing. This site is located between the north third ring road and north fourth ring road, and the Beijing–Tibet motorway is on the eastern side. The geographic location of the station is  $39.97^{\circ}$  N,  $116.37^{\circ}$  E, and the elevation is approximately 60 m.

20 The instrument used to observe the MLH was a single-lens ceilometer CL31 (Vaisala). This instrument utilizes pulsed diode laser lidar technology (910 nm waveband) to measure the attenuated backscatter coefficient profile of atmospheric aerosols and then determine the MLH. In practical measurements using the CL31, the time resolution was set to 16 s, the vertical resolution was set to 10 m, and the measurement range was

25 7.7 km. Because the atmospheric aerosol concentration is relatively high in Beijing, the CL31 lens was cleaned with clear water every 3 days. The conventional meteorological

[Title Page](#)

[Abstract](#)

[Introduction](#)

[Conclusions](#)

[References](#)

[Tables](#)

[Figures](#)

[◀](#)

[▶](#)

[◀](#)

[▶](#)

[Back](#)

[Close](#)

[Full Screen / Esc](#)

[Printer-friendly Version](#)

[Interactive Discussion](#)



data during the same period were from temperature, humidity, wind speed, and wind direction observations at 8, 15, 32, 47, 65, 80, 100, 120, 140, 160, 180, 200, 240, 280, and 320 m up the tower, and the temporal resolution was 5 min. A detailed description is provided by Song et al. (2013). The thermodynamic parameter data in the atmospheric mixing layer (sensible heat, latent heat, radiation, friction velocity, etc.) during the same period were from ultrasonic anemometers at 47, 140 and 280 m on the meteorological tower, and the time resolution was 5 min. A detailed description is provided by Song and Wang (2012). The observation data of PM<sub>2.5</sub> and PM<sub>10</sub> during the same period were from Thermo Electric Inc. (RP1400a), and the time resolution was 5 min.

5 A detailed description is provided by Liu et al. (2014).

The meteorological sounding profile data were measured by the international standard weather station (ID: ZBAA), which is located outside the south second ring road in the Fengtai district, Beijing, 10 km from the station on the tower of the Institute of Atmospheric Physics. The geographic position of station ZBAA is 39.48° N and 116.28° E, and the elevation (a.s.l.) is approximately 34 m. The meteorological sounding profile data observed at station ZBAA included two categories: conventional observations, which were conducted at 08:00 LT in the morning and 20:00 LT in the evening; and intensified observations, which were conducted at 14:00 LT in the afternoon every Thursday. The observed meteorological parameters included atmospheric pressure, temperature, wind speed, wind direction, and humidity. According to the classification method of Eresmaa et al. (2006), we defined all of the meteorological sounding profiles as a convection state when they exhibited negative lapse rates for the virtual potential temperature within 200 m and bulk Richardson number within 100 m, and the other profiles were defined as a stable state. We obtained 260 and 540 effective observation samples for the two types of weather conditions, respectively. In order to characterize the degree of the air pollution in Beijing, visibility at station ZBAA was obtained from the web page of Wyoming Engineering University (<http://weather.uwyo.edu>).

<a href="#">Title Page</a>	
<a href="#">Abstract</a>	<a href="#">Introduction</a>
<a href="#">Conclusions</a>	<a href="#">References</a>
<a href="#">Tables</a>	<a href="#">Figures</a>
<a href="#">◀</a>	<a href="#">▶</a>
<a href="#">◀</a>	<a href="#">▶</a>
<a href="#">Back</a>	<a href="#">Close</a>
<a href="#">Full Screen / Esc</a>	
<a href="#">Printer-friendly Version</a>	
<a href="#">Interactive Discussion</a>	



## 2.2 Determination of the MLH

### 2.2.1 MLH retrieval by ceilometer

Because the lifetime of particles is relatively long and could be several days or even weeks, the distribution of particle concentrations inside the atmospheric mixing layer is even more uniform compared with that of gaseous pollutants. However, the particle concentration in the mixing layer and free atmosphere is significantly different. By analysing the attenuated backscatter coefficient profile of atmospheric particles, the position at which a sudden change occurs in the attenuated backscatter coefficient is the top of the atmospheric mixing layer. In this study, we used the gradient method to determine the MLH by selecting the location with the maximum negative gradient ( $-d\beta/dx$ ) in the attenuated backscatter coefficient profile diagram for the aerosol as the top of the mixing layer (Steyn, et al., 1999). To eliminate the inherent noise and aerosol layer structure influence on the data, spatial and temporal averaging must be applied before the gradient method can be used to calculate the MLH from the profile data (Münkel et al., 2007; Tang et al., 2015).

### 2.2.2 MLH retrieval by radiosonde

A number of methods have been developed to analyse the mixing layer through the meteorological sounding profile (Beyrich, 1997; Sibert et al., 2000; Wang and Wang, 2014). In this study, we calculated the MLH for the convective state and stable state, respectively. For the convective state, we used the Holzworth method (Holzworth, 1964, 1967), which is most widely applied to obtain the MLH by analysing variations in the virtual potential temperature. In a stable state, a low-level jet often occurs in the Beijing area, and we can determine the MLH by analysing the position of the low-level jet (Tang et al., 2015). If the low-level jet does not occur under stable weather conditions, the altitude where the Richardson number is greater than 1 is the MLH (Vogelezang and Holtslag, 1996; Eresmaa et al., 2006).

Title Page

Abstract

Introduction

Conclusions

References

Tables

Figures

|◀

▶|

◀

▶

Back

Close

Full Screen / Esc

Printer-friendly Version

Interactive Discussion



**Mixing layer height  
and air pollution over  
Beijing**

G. Tang et al.

[Title Page](#)[Abstract](#)[Introduction](#)[Conclusions](#)[References](#)[Tables](#)[Figures](#)[|◀](#)[▶|](#)[◀](#)[▶](#)[Back](#)[Close](#)[Full Screen / Esc](#)[Printer-friendly Version](#)[Interactive Discussion](#)

### 3 Results and discussions

#### 3.1 Verification of the MLH

Previous observation studies using ceilometers could not resolve issues with applying ceilometers in Chinese areas with high aerosol concentrations. In this study, the methods of Eresmaa et al. (2006) and Münkel et al. (2007) were used to divide the samples into stable and convective states according to the atmospheric stratification status. The MLH data acquired by meteorological sounding profiles and the ceilometer were compared (Fig. 2), and the results were evaluated. The comparative analysis showed that the MLH observed by the ceilometer was overestimated and underestimated in a portion of the samples. Because the ceilometer determines the MLH by measuring the attenuated backscatter profile of atmospheric particles, if the concentration of atmospheric particles is relatively low, then the height measurement errors of the mixing layer will increase correspondingly (Eresmaa et al., 2006; Muñoz and Undurraga, 2010). An analysis of the relationship between the visibility and comparison results showed that underestimations in the ceilometer observation results generally corresponded with good visibility and low aerosol concentrations. Nevertheless, among the samples with relatively good visibility, a number of samples had relatively low errors (Fig. 2). Consequently, low pollution and good visibility are not sufficient conditions to predict underestimations in the observation results.

To investigate why ceilometer results produced underestimations, we analysed cases with low aerosol concentrations and small measurement errors and found that when there was a large difference in the aerosol concentration between the near surface and high altitude, the calculation error of the MLH decreased, even if the aerosol concentration was relatively low. By further analysing the relationship between the ceilometer and meteorological sounding profile results with the relative humidity and wind vectors, we found that ceilometer underestimations corresponded with low relative humidity and large wind speed, with winds mostly from the north (Figs. 3 and 4). The local meteorological conditions in Beijing indicated that this type of meteorological condition is usu-

[Title Page](#)[Abstract](#)[Introduction](#)[Conclusions](#)[References](#)[Tables](#)[Figures](#)[◀](#)[▶](#)[◀](#)[▶](#)[Back](#)[Close](#)[Full Screen / Esc](#)[Printer-friendly Version](#)[Interactive Discussion](#)

ally caused by a bypass of a cold air mass. When strong northerly winds are dominant over Beijing, dry and clear air masses prevail, and the large wind speed causes the atmospheric aerosols to rapidly spread to the downstream region, resulting in a dramatic decrease of aerosol concentration. In addition, the low humidity of the air mass suppresses the liquid-phase and heterogeneous reactions for the gaseous precursors of aerosol, and the hygroscopic growth of aerosols can also be neglected. Therefore, the aerosol generation velocity is much lower than the loss rate because of transportation, leading to low aerosol concentrations and uniform vertical gradients. Once the aerosol concentrations in vertical direction become uniform, the ceilometer cannot calculate the MLH through sudden changes in the attenuated backscatter profile, which results in serious underestimations. An analysis of the relationship between the Richardson number and the error shows that when the ceilometer-measured MLH is subject to relatively large errors, the Richardson number is approximately 0. Therefore, the near-neutral atmospheric stratification that occurs when a cold air mass passes through is the main cause for the serious underestimation in the observation results by the ceilometer.

To investigate the overestimations in the ceilometer results, an analysis of the observation results for the particle concentration showed that in this situation, the PM<sub>2.5</sub> concentration is relatively low, but the PM<sub>10</sub> concentration is relatively high (Fig. 2). To investigate the reason of the overestimations, we used the meteorological sounding profile at 14:00 LT on 19 December 2009 as an example and analysed it for overestimations (Fig. 5). This profile exhibited an obvious bi-level structure, with the first level at approximately 1100 m; where the virtual potential temperature begins to gradually increase, the wind speed begins to increase, and the ozone concentration is transported from the background area with a concentration of about 40 ppbv. The second level is at approximately 1600 m, where the variation rate of virtual potential temperature increases. However, the ceilometer-measured attenuated backscatter coefficient profile cannot resolve this type of bi-level structure. A PM<sub>2.5</sub>/PM<sub>10</sub> ratio of only 0.15 exhibits clear characteristics of dust crossing. Therefore, the aerosol concentration caused by

this type of dust crossing is uniform in the vertical direction below the second layer for the ceilometer, whereas the presence of obvious wind shear and sudden virtual potential temperature changes for the radiosondes are the main reasons for the overestimated observation results by the ceilometers (Figs. 2 and 5).

After determining the reasons for the underestimations and overestimations in the ceilometer data, the results with large errors according to certain principles must be eliminated. For underestimations, the meteorological data at the observation station were used to eliminate time periods of crossing cold air when the temperature and wind velocity are subject to a sudden change. For overestimations, we used the date of dust occurrence based on the sand–dust weather almanac to eliminate the time periods of dust crossing when the ratio of  $\text{PM}_{2.5}$  and  $\text{PM}_{10}$  suddenly decreases. An analysis of the meteorological sounding profiles after eliminating the erroneous data showed that a high correlation occurred between the post-elimination ceilometer data and meteorological sounding observations, and the correlation coefficient was more than 0.9, which also demonstrated the effectiveness and manipulability of the elimination method (Fig. 6). Overall, by analysing the weather conditions that caused the error of ceilometer observation, the conventional meteorological data and  $\text{PM}_{2.5}$  and  $\text{PM}_{10}$  were used to eliminate the observation results. The elimination results are good, and this method replaces the time-consuming method of filtering the data manually, which is of great practical value for future measurements of MLH with ceilometers.

### 3.2 MLH variations

To provide a detailed description of variations in the MLH, we selected high-quality MLH and meteorological data in 3 consecutive years (from December 2009 to November 2012). First, the effectiveness of the data must be verified after performing the elimination by the aforementioned method. The results of the evaluation indicate that the effectiveness of the data in different seasons is significantly negatively correlated with wind speed and significantly positively correlated with relative humidity (Fig. 7a). For spring and winter seasons with relatively large wind speeds and relatively low hu-

[Title Page](#)[Abstract](#)[Introduction](#)[Conclusions](#)[References](#)[Tables](#)[Figures](#)[|◀](#)[▶|](#)[◀](#)[▶](#)[Back](#)[Close](#)[Full Screen / Esc](#)[Printer-friendly Version](#)[Interactive Discussion](#)

**Mixing layer height  
and air pollution over  
Beijing**

G. Tang et al.

[Title Page](#)[Abstract](#)[Introduction](#)[Conclusions](#)[References](#)[Tables](#)[Figures](#)[|◀](#)[▶|](#)[◀](#)[▶](#)[Back](#)[Close](#)[Full Screen / Esc](#)[Printer-friendly Version](#)[Interactive Discussion](#)

especially for weather with dry wind and relatively high MLHs, the monthly means of MLH in winter and spring seasons were likely underestimated. To avoid the influence of data elimination on the study, we analysed the relationship between daily changes of the mixing layer and the sensible heat flux and found that the average MLH from 12:00 to 17:00 LT and the sensible heat flux were well correlated and had a correlation coefficient of 0.65, which characterizes the dominant role of radiation in the variations of MLH (Fig. 8).

### 3.3 Impact of mountainous plain winds on MLH

We analysed the diurnal variations in MLH on a monthly basis and found that the MLH develops in four stages: from 09:00 to 14:00 LT, which is the fast development stage for the MLH; from 14:00 to 18:00 LT, which is the maintenance stage of the mixing layer; from 18:00 to 20:00 LT, which is the rapid decrease stage of the mixing layer; and after 20:00 LT and until 08:00 LT in the morning of the second day, which is the stable boundary layer stage with relatively low MLH (Fig. 9a). These types of development and dissipation mechanisms are consistent with the description of Stull (1988). Although the daily average MLH is close between spring and summer, the diurnal variation in the MLH exhibits considerable differences. At night-time in spring, the MLH is high and relatively stable, whereas at night-time in summer, the MLH exhibits a gradual decreasing trend. After sunrise and before 12:00 LT, the growth rate of the atmospheric MLH is relatively high in spring and reaches  $114 \text{ m h}^{-1}$ , whereas the hourly growth rate of the mixing layer is relatively low in summer and only reaches  $102 \text{ m h}^{-1}$ . Between 12:00 and 14:00 LT in spring, the growth rate of the MLH is  $119 \text{ m h}^{-1}$ , whereas the growth rate of the MLH is significantly enhanced in summer and reaches  $165 \text{ m h}^{-1}$ . Such changes reflect the convex variation characteristics in spring and concave characteristics in summer during the development stage of the MLH.

According to the description in Sect. 3.2, variations in the MLH should exhibit a good linear relationship with the amount of radiation. Because of the relatively high radiation in spring, the relatively high MLH variation for days with lower radiation in summer is

<a href="#">Title Page</a>	
<a href="#">Abstract</a>	<a href="#">Introduction</a>
<a href="#">Conclusions</a>	<a href="#">References</a>
<a href="#">Tables</a>	<a href="#">Figures</a>
<a href="#">◀</a>	<a href="#">▶</a>
<a href="#">◀</a>	<a href="#">▶</a>
<a href="#">Back</a>	<a href="#">Close</a>
<a href="#">Full Screen / Esc</a>	
<a href="#">Printer-friendly Version</a>	
<a href="#">Interactive Discussion</a>	



difficult to explain with the radiation flux, which indicates that there are other factors that affect the characteristics of the MLH variation. Because the MLH is affected by many factors, its development is mainly related to the magnitude of turbulent energy. Two components are closely related to turbulent energy: the heat flux caused by radiation and the momentum flux generated by wind shear (Stull, 1988). Because the seasonal variation of heat flux is difficult to explain according to the aforementioned criteria, we analysed the seasonal variations in the horizontal wind vector at Beijing station. To avoid the impact of near-surface buildings on the wind measurements, we selected the wind vector at 100 m on the Beijing tower. Figure 9b shows that there is an obvious seasonal variation in the wind vector of the Beijing area. The winter season is dominated by a northwesterly wind, whereas the spring season exhibits a northwesterly wind in the morning and southwesterly wind in the afternoon. What matters most is that the alternation phenomenon between the mountainous wind beginning at 03:00 LT at night and the valley wind at 12:00 LT in the afternoon starts to occur in summer. From September, the circulation of mountainous plain wind slowly weakens, and this regional circulation essentially disappears in November. Beijing is affected by the Siberian High in winter and spring, a prevailing northwest wind and dry air mass with relatively large wind velocity occur. However, the northward lift and westward intrusion of a subtropical high in summer causes the southerly moist air mass with relatively small wind velocity to dominate. Because Beijing is located to the west of the Taihang Mountains and south of the Yanshan Mountains, in the absence of large- or medium-scale meteorological systems passing through in summer, the local mountainous plain wind is superimposed to the southerly air flow and jointly affects the meteorological characteristics of the North China Plain. When this regional circulation occurs along with surface cooling at night in summer, the cold air near the surface forms a shallow down-sliding flow from the northeast to the southwest, and this is called the downslope wind or cold drainage flow. The cooled air then flows into the plain and accumulates in a cold pool, and the cold air that continuously fills the plain continues to increase the thickness of the inversion layer, and the thickness of the mixing layer gradually de-

<a href="#">Title Page</a>	
<a href="#">Abstract</a>	<a href="#">Introduction</a>
<a href="#">Conclusions</a>	<a href="#">References</a>
<a href="#">Tables</a>	<a href="#">Figures</a>
<a href="#">◀</a>	<a href="#">▶</a>
<a href="#">◀</a>	<a href="#">▶</a>
<a href="#">Back</a>	<a href="#">Close</a>
<a href="#">Full Screen / Esc</a>	
<a href="#">Printer-friendly Version</a>	
<a href="#">Interactive Discussion</a>	



<a href="#">Title Page</a>	
<a href="#">Abstract</a>	<a href="#">Introduction</a>
<a href="#">Conclusions</a>	<a href="#">References</a>
<a href="#">Tables</a>	<a href="#">Figures</a>
<a href="#">◀</a>	<a href="#">▶</a>
<a href="#">◀</a>	<a href="#">▶</a>
<a href="#">Back</a>	<a href="#">Close</a>
<a href="#">Full Screen / Esc</a>	
<a href="#">Printer-friendly Version</a>	
<a href="#">Interactive Discussion</a>	

creases. After sunrise as the radiation enhances, the impact of thermal buoyancy lift causes the MLH to increase rapidly, and this type of cold drainage flow is maintained until 12:00 LT. After 12:00 LT, the plain wind in the southwesterly direction gradually dominates and is maintained until approximately 03:00 LT in the morning of the second day. According to Fig. 9c, from 03:00 LT to 12:00 LT during summer, the air space from the near surface to 300 m is gradually controlled by the cold drainage flow in the northeasterly direction, and the MLH exhibits a gradually diminishing trend from 03:00 to 06:00 LT. This trend does not occur in spring (Fig. 9a). Similarly, between 09:00 and 12:00 LT, the cold drainage flow causes a low hourly growth rate of the mixing rate in summer, whereas the growth rate of the MLH is high in spring. After 12:00 LT, the southerly plain wind causes the growth rate of the MLH to increase from 12:00 to 14:00 LT in summer. The gradual reduction of the night-time mixing layer and the relatively low rising velocity after sunrise demonstrate the inhibitory effect of this cold drainage flow on the development of the MLH. In summary, the mountainous wind in summer causes the mixing layer to gradually decline at night, which suppresses the development of the mixing layer before noon, and the prevalence of plain winds after noon causes the mixing layer to increase rapidly. Therefore, this regional circulation leads to the concave-down variation in the fast development stage of the mixing layer in summer compared to the spring.

## 20 3.4 Implications for air pollution

### 3.4.1 Thermal/dynamic structures inside mixing layers with different degrees of pollution

To analyse variations in the thermal dynamic parameters inside atmospheric mixing layers under different degrees of pollution, visibility was used to indicate the degree of atmospheric pollution. Variations in atmospheric visibility were used in the statistical analysis of the thermal dynamic parameters in the atmospheric mixing layer, and variation features were obtained for the wind speed, humidity, sensible heat, latent heat, fric-



[Title Page](#)[Abstract](#)[Introduction](#)[Conclusions](#)[References](#)[Tables](#)[Figures](#)[|](#)[|](#)[◀](#)[▶](#)[Back](#)[Close](#)[Full Screen / Esc](#)[Printer-friendly Version](#)[Interactive Discussion](#)

tion velocity, and turbulent kinetic energy (TKE) at 280 m under different visibility conditions. As shown in Fig. 10, on clear days with atmospheric visibility  $\geq 10$  km, the relative humidity was the lowest, with an average of 43.3 %, whereas the sensible heat flux, friction velocity and TKE were the highest and averaged  $20.4 \text{ W m}^{-2}$ ,  $0.45 \text{ m s}^{-1}$ , and  $0.99 \text{ m}^2 \text{s}^{-2}$ , respectively. The MLH was 664.2 m on average, and the maximum after noon could reach 1144.8 m. With declines of atmospheric visibility, slight haze pollution occurred in the visibility range of 5 to 10 km (CMA, 2010). Compared with clear days, the relative humidity during light haze pollution significantly increased to 63.1 %, and both the friction velocity and TKE significantly declined to  $0.32 \text{ m s}^{-1}$  and  $0.64 \text{ m}^2 \text{s}^{-2}$ , respectively, at a reduction rate of approximately 30 %, whereas the average sensible heat flux and MLH did not show significant changes at values of  $19.7 \text{ W m}^{-2}$  and 671.0 m, respectively. As the atmospheric visibility continued to decline, light haze pollution occurred in the visibility range of 3 to 5 km, medium haze pollution occurred in the visibility range of 2 to 3 km, and heavy haze pollution occurred in the visibility range of less than 2 km (CMA, 2010). Compared with slight haze pollution conditions, the relative humidity continued to increase with the aggravated pollution, and in the periods of light, medium and heavy haze it could reach to 73.4, 79.6, and 86.4 %, respectively; the friction velocity was 0.28, 0.26, and  $0.23 \text{ m s}^{-1}$ , respectively; the TKE was 0.56, 0.52, and  $0.46 \text{ m}^2 \text{s}^{-2}$ , respectively; the sensible heat flux was 15.2, 12.8, and  $7.8 \text{ W m}^{-2}$ , respectively; and the MLH was 586.1, 430.0, and 320.1 m, respectively. Therefore, when clear days change to slight haze, the wind speed, friction velocity, and TKE significantly decline but the sensible heat flux and MLH do not change significantly. When the degree of pollution transforms from slight haze to light, medium, and heavy haze, significant changes do not occur in the friction velocity and TKE, the sensible heat flux significantly declines, and the MLH gradually decreases. It should be noted that although the relative humidity varied considerably at different pollution stages, significant differences did not occur in the latent heat flux, which varied from clear days to heavy haze days at 18.7, 19.9, 21.5, 18.8, and  $19.8 \text{ W m}^{-2}$ . Thus, when clear days transform to slight haze, dynamic effects have a relatively large influence on the mixing

layer, whereas thermodynamic effects have a relatively significant influence during the transition process from slight haze to heavy haze.

To verify these results, we examined the TKE budget equation. If we presume a horizontal average and neglect the advection of wind, then the forecast equation of the  
5 TKE can be written as follows (Garratt, 1992):

$$\frac{\partial \bar{e}}{\partial t} = -\overline{u'w'} \frac{\partial \bar{u}}{\partial z} + \frac{\partial g}{\partial \theta_v} \overline{w'\theta'_v} - \frac{\partial \left( \overline{w'e} + \frac{\overline{w'p'}}{\rho} \right)}{\partial z} - \varepsilon, \quad (1)$$

where  $\theta_v$  is the virtual potential temperature. The first term on the right side of the equation is the production and loss term caused by wind shear, the second term on the right side of the equation is the buoyancy production and depletion term, the third

10 term on the right side of the equation is the turbulent transport and pressure-related term, and the last term on the right side of the equation is the dissipation term. The turbulent transportation term does not generate or destroy the TKE, and it just moves the TKE from one position to another position or redistributes the TKE. This term remains constant at zero in the entire mixing layer; therefore, we did not analyse it in

15 this study. Moreover, because the time period of pollution usually corresponds to the stable state, the pressure-related term is also small at this time. Therefore, to differentiate the contribution of horizontal turbulence and vertical turbulence to the TKE, we only analysed the shear and buoyancy term in TKE forecast equation (Ye et al., 2015). As shown in Fig. 10d, the average value of the buoyancy term for clear days,

20 slight haze, light haze, medium haze, and heavy haze is  $0.67 \times 10^{-3}$ ,  $0.64 \times 10^{-3}$ ,  $0.49 \times 10^{-3}$ ,  $0.39 \times 10^{-3}$ , and  $0.24 \times 10^{-3} \text{ m}^2 \text{s}^{-3}$ , respectively, and the average shear term is  $1.02 \times 10^{-3}$ ,  $0.66 \times 10^{-3}$ ,  $0.37 \times 10^{-3}$ ,  $0.26 \times 10^{-3}$ , and  $0.23 \times 10^{-3} \text{ m}^2 \text{s}^{-3}$ , respectively. Therefore, the key meteorological factor for the conversion from clear days to slight haze is the shear term in TKE, and it is mainly characterized by a significant reduction of horizontal wind velocity; the key meteorological factor for the conversion

[Title Page](#)[Abstract](#)[Introduction](#)[Conclusions](#)[References](#)[Tables](#)[Figures](#)[◀](#)[▶](#)[◀](#)[▶](#)[Back](#)[Close](#)[Full Screen / Esc](#)[Printer-friendly Version](#)[Interactive Discussion](#)

from slight haze to light, medium, and heavy haze is the buoyancy term in TKE, and it is mainly characterized by a significant reduction of the sensible heat and the MLH.

### **3.4.2 Critical meteorological conditions for the formation and dissipation of heavy air pollution**

- 5 Variations in the MLH represent the vertical diffusion capability of pollutants, and higher mixing layers indicate a stronger vertical diffusion capability. Variations in the wind speed represent the horizontal diffusion capability of pollutants, and higher wind speeds indicate a stronger horizontal diffusion capability. In most studies, the product of the MLH and the wind speed (ventilation coefficient) is usually used as the index  
10 to measure the capability of atmospheric diffusion (Tang et al., 2015). To represent the atmospheric diffusion capability during different seasons, we analysed the ventilation coefficient (VC) in the Beijing area. As shown in Fig. 11a, the atmospheric diffusion capability is the strongest in spring with a ventilation coefficient of approximately  $2000 \text{ m}^2 \text{ s}^{-1}$ ; the atmospheric diffusion capability in summer reaches  $1782 \text{ m}^2 \text{ s}^{-1}$ , and in autumn and winter, it reaches  $1095$  and  $1072 \text{ m}^2 \text{ s}^{-1}$ , respectively. The ventilation coefficient is the highest and the lowest in April and December when the maximum and minimum are  $2074$  and  $893 \text{ m}^2 \text{ s}^{-1}$ , respectively. The ventilation coefficient in April is 2.3 times than that in December. Although the atmospheric diffusion capability is strong in spring and summer and the atmospheric diffusion capability in summer is 1.7  
15 times than that of autumn and winter, the visibility is the lowest ( $\sim 9 \text{ km}$ ) in summer and the  $\text{PM}_{2.5}$  concentration is the highest ( $\sim 85 \mu\text{g m}^{-3}$ ) (Fig. 11a). By dividing the visibility between  $\geq 10 \text{ km}$  and  $< 10 \text{ km}$ , we find that the occurrence frequency of haze is highest in summer at up to 73 %, and approximately 40 % in other seasons. Therefore,  
20 the heavy pollution in summer and its relatively high atmospheric diffusion capability exhibit a conflicted state.  
25

According to the discussion in Sect. 3.4.1, small differences occur in the atmospheric MLH between slight haze days and clear days. As the haze grade increases, the atmospheric MLH gradually declines, which indicates that at a slight pollution stage, the



**Mixing layer height  
and air pollution over  
Beijing**

G. Tang et al.

degree of atmospheric pollution is essentially not related to the MLH and the pollution degree depends on the horizontal diffusion capability as affected by the horizontal wind speed. At the heavy pollution stage, the pollution degree is determined by the vertical diffusion capability as affected by the MLH. The statistical results of previous studies indicate that as the MLH decreases and the concentration of atmospheric particles gradually increases, the visibility gradually decreases. However, an analysis of the MLH and the particle concentration or visibility indicates that the correlation between the MLH and the particle concentration or visibility is not strong, and they may even be uncorrelated (Li et al., 2015; Tang et al., 2015). To determine the relationship between the atmospheric MLH and atmospheric pollution, we analysed the correlation between the daily average MLH and atmospheric visibility and found that the correlation between the MLH and atmospheric visibility is poor and has a correlation coefficient of 0.08, which is consistent with the results of previous studies (Li et al., 2015). However, an analysis of the correlation between the MLH and visibility under different relative humidity showed that when the relative humidity is greater than 80 %, the correlation between the MLH and visibility suddenly increases and produces a correlation coefficient of 0.72 (Fig. 11b). Previous studies have indicated that there are considerable differences in the chemical composition of particles between clear and haze days, and as the particle concentration increases, the magnitude of enhancement is highest for sulfates, nitrates, and ammonium aerosols with relatively strong hygroscopicity, whereas the magnitude of enhancement is relatively low for organic matter aerosols with relatively weak hygroscopicity. Therefore, the variation in crustal elements is not significant and exhibits higher sulfate, nitrate, and ammonium ratios on haze days (Zhang et al., 2014). This result also indicates that the humidity plays an important role in transforming the pollutants for heavy haze days. Under low humidity conditions, the contribution of humidity-related physiochemical processes to the atmospheric particles is relatively low, and the processes of local emissions, regional transportation, and physiochemical generation dominate the concentration of atmospheric particles. Therefore, the correlation between visibility and the MLH is insignificant because of the contributions of parti-

[Title Page](#)[Abstract](#)[Introduction](#)[Conclusions](#)[References](#)[Tables](#)[Figures](#)[◀](#)[▶](#)[◀](#)[▶](#)[Back](#)[Close](#)[Full Screen / Esc](#)[Printer-friendly Version](#)[Interactive Discussion](#)

<a href="#">Title Page</a>	
<a href="#">Abstract</a>	<a href="#">Introduction</a>
<a href="#">Conclusions</a>	<a href="#">References</a>
<a href="#">Tables</a>	<a href="#">Figures</a>
<a href="#">◀</a>	<a href="#">▶</a>
<a href="#">◀</a>	<a href="#">▶</a>
<a href="#">Back</a>	<a href="#">Close</a>
<a href="#">Full Screen / Esc</a>	
<a href="#">Printer-friendly Version</a>	
<a href="#">Interactive Discussion</a>	



cles from different processes. Under high humidity conditions, the influence of regional transportation during heavy pollution periods may worsen the correlation between the heavy pollution degree and the MLH. Therefore, a relatively strong correlation indicates that heavy pollution is mainly from local contributions, which is consistent with the previous study (Tang et al., 2015). Increases in relative humidity cause an increase in the amount of liquid-phase and heterogeneously generated chemicals and significant hygroscopic growth of particles, and the main source of particle changes to locally generated humidity-related physiochemical processes. Overall, the high correlation between visibility and the MLH under high humidity characterizes the generation of humidity-related physiochemical processes as the main source of atmospheric particles under heavy pollution, whereas the dissipation of atmospheric particles mainly depends on the vertical diffusion capability, which is dominated by the atmospheric MLH. These analyses show that the primary critical condition for the formation of heavy pollution is relative humidity, and the critical threshold is 80 %. To determine the other critical condition for the MLH, we analysed the fitting equation during heavy haze periods when the relative humidity exceeds 80 % and calculated the MLH corresponding to four different degrees of pollution with atmospheric visibility of 2, 3, 5, and 10 km. We found that the critical MLH for the four states of slight, light, medium, and heavy haze were 1209, 618, 382, and 263 m, respectively. This result demonstrates the two critical meteorological conditions for the formation of heavy pollution and is significant for the forecasting and warning of atmospheric pollution.

After determining the critical meteorological condition for the formation of heavy pollution, an analysis of the meteorological conditions in summer showed that the relatively low wind speed is a prerequisite for an increase in haze days and the high relative humidity increases the generation velocity of particles (Fig. 7a). Once the cloud fraction increases, radiation levels will dramatically decline, and the atmospheric MLH will also decrease as well. Such conditions cause a weakening of the atmospheric diffusion capability and lead to the frequent occurrence of heavy pollution events with an enhanced concentration of atmospheric particles and reduced visibility.

## 4 Conclusions

Continuous high-resolution observations of MLH are required to understand the structure of the atmospheric mixing layer in the Beijing and North China Plain areas. In order to acquire the high-resolution observations of MLH, a study was performed from

- 5 July 2009 to December 2012 using a ceilometer in the Beijing urban area. Based on a comparison and validation of multiple types of data, we determine that the ceilometer underestimates MLH during neutral stratification caused by strong winds, whereas it overestimates MLH during dust crossing. By combining conventional meteorological data and PM<sub>2.5</sub> and PM<sub>10</sub> observational data, we screen the observation results for  
10 the MLH, and the ceilometer observations are fairly consistent with the meteorological radiosonde profile results. The correlation coefficient is more than 0.9, and the effective rate of acquired data is near 80 %. This method replaces the time-consuming method of filtering the data manually, which is of great practical value for future measurements of MLH with ceilometers.

- 15 The characteristics of variation in the MLH indicate that the MLH in the Beijing area exhibits the feature of being low in autumn and winter, and being high in spring and summer. There is a significant correlation between the variation in the MLH and the sensible heat flux, which characterizes the dominant role of radiation in the variations of MLH. However, the characteristics of diurnal variation in the mixing layer during  
20 summer is affected by the circulation of mountainous plain winds. The mountainous wind in summer causes the mixing layer at night to gradually decline, which suppresses the development of the mixing layer before noon, and the prevalence of plain winds after noon causes the mixing layer to increase rapidly. Therefore, the mountainous plain winds leads to the concave-down variation in the fast development stage of the mixing layer in summer compared to the spring.

25 By applying visibility as the index for the classification of atmospheric pollution degree, it is found that in comparison with a clear day, the variation of sensible heat and buoyancy term in TKE of a slight haze day is insignificant, and the reduction of shear

<a href="#">Title Page</a>	
<a href="#">Abstract</a>	<a href="#">Introduction</a>
<a href="#">Conclusions</a>	<a href="#">References</a>
<a href="#">Tables</a>	<a href="#">Figures</a>
<a href="#">◀</a>	<a href="#">▶</a>
<a href="#">◀</a>	<a href="#">▶</a>
<a href="#">Back</a>	<a href="#">Close</a>
<a href="#">Full Screen / Esc</a>	
<a href="#">Printer-friendly Version</a>	
<a href="#">Interactive Discussion</a>	



term in TKE is significant; in comparison with the slight haze day, the variation of shear term in TKE of medium and heavy haze days is insignificant, and the declination of sensible heat and buoyancy term in TKE is significant. At a slight pollution stage, the degree of atmospheric pollution is essentially not related to the MLH and the pollution degree depends on the horizontal diffusion capability as affected by the horizontal wind speed. At the heavy pollution stage, the pollution degree is determined by the vertical diffusion capability as affected by the MLH. Although the correlation between the daily MLH and the visibility is very poor, the correlation between them is significantly enhanced as the relative humidity increases. The high correlation between visibility and the MLH under high humidity characterizes the generation of humidity-related physiochemical processes as the source of atmospheric particles under heavy pollution, whereas the dissipation of atmospheric particles mainly depends on the vertical diffusion capability, which is dominated by the atmospheric MLH.

The aforementioned results provide reliable basic data for better portraying the structure of the boundary layer and improving the parameterization scheme of the boundary layer in meteorological models. Studies on the atmospheric mixing layer and its thermal dynamic structure under different degrees of pollution reveal the critical meteorological conditions underlying the formation, evolution, and dissipation of atmospheric heavy pollution, and provide a scientific basis for improving atmospheric chemistry models and the forecasting and warning of atmospheric pollution.

**Acknowledgements.** This work was supported by the CAS Strategic Priority Research Program Grant (no. XDB05020000 and XDA05100100) and National Natural Science Foundation of China (nos. 41230642 and 41222033).

[Title Page](#)[Abstract](#)[Introduction](#)[Conclusions](#)[References](#)[Tables](#)[Figures](#)[◀](#)[▶](#)[◀](#)[▶](#)[Back](#)[Close](#)[Full Screen / Esc](#)[Printer-friendly Version](#)[Interactive Discussion](#)

## References

## Mixing layer height and air pollution over Beijing

G. Tang et al.

- Aron, R.: Mixing height – an inconsistent indicator of potential air pollution concentrations, *Atmos. Environ.*, 17, 2193–2197, 1983.
- Barbara, H. and Andrea, L.: Determination of the atmospheric boundary layer height from radiosonde and lidar backscatter, *Bound.-Lay. Meteorol.*, 120, 181–200, 2006.
- Beyrich, F.: Mixing height estimation from SODAR data – a critical discussion, *Atmos. Environ.*, 31, 3941–3953, 1997.
- Chen, W., Kuze, H., Uchiyama, A., Suzuki, Y., and Takeuchi, N.: One-year observation of urban mixed layer characteristics at Tsukuba, Japan using a micro pulse lidar, *Atmos. Environ.*, 35, 4273–4280, doi:10.1016/S1352-2310(01)00181-9, 2001.
- Chen, Y., Zhao, C., Zhang, Q., Deng, Z., Huang, M., and Ma, X.: Aircraft study of Mountain Chimney Effect of Beijing, China, *J. Geophys. Res.*, 114, D08306, doi:10.1029/2008JD010610, 2009.
- Chen, Z., Liu, W., Zhang, Y., He, J., and Ruan, J.: Mixing layer height and meteorological measurements in Hefei China during the total solar eclipse of 22 July, 2009, *Opt. Laser Technol.*, 43, 50–54, doi:10.1016/j.optlastec.2010.04.022, 2011.
- China Meteorological Administration (CMA): Observation and forecasting levels of haze, QX/T 113-2010, Beijing, 2010.
- Devara, P. C. S., Ernest, R. P., Murthy, B. S., Pandithurai, G., Sharma, S., and Vernekar, K. G.: Intercomparison of nocturnal lower-atmospheric structure observed with LIDAR and SODAR techniques at Pune, India, *J. Appl. Meteorol.*, 34, 1375–1383, 1995.
- Ding, G. A., Chen, Z. Y., Gao, Z. Q., Yao, W. Q., Li, Y., Cheng, X. H., Meng, Z. Y., Yu, H. Q., Wong, K. H., Wang, S. F., and Miao, Q. J.: Vertical structures of PM<sub>10</sub> and PM<sub>2.5</sub> and their dynamical character in low atmosphere in Beijing urban areas, *Sci. China Ser. D*, 35, 31–44, 2005.
- Emeis, S. and Schäfer, K.: Remote sensing methods to investigate boundary-layer structures relevant to air pollution in cities, *Bound.-Lay. Meteorol.*, 121, 377–385, 2006.
- Emeis, S., Münkel, C., Vogt, S., Müller, W. J., and Schäfer, K.: Atmospheric boundary-layer structure from simultaneous SODAR, RASS, and ceilometer measurements, *Atmos. Environ.*, 38, 273–286, 2004.

<a href="#">Title Page</a>	
<a href="#">Abstract</a>	<a href="#">Introduction</a>
<a href="#">Conclusions</a>	<a href="#">References</a>
<a href="#">Tables</a>	<a href="#">Figures</a>
<a href="#">◀</a>	<a href="#">▶</a>
<a href="#">◀</a>	<a href="#">▶</a>
<a href="#">Back</a>	<a href="#">Close</a>
<a href="#">Full Screen / Esc</a>	
<a href="#">Printer-friendly Version</a>	
<a href="#">Interactive Discussion</a>	



- Emeis, S., Jahn, C., Münkel, C., Münsterer, C., and Schäfer, K.: Multiple atmospheric layering and mixing-layer height in the Inn valley observed by remote sensing, *Meteorol. Z.*, 16, 415–424, 2007.
- Emeis, S., Schäfer, K., and Münkel, C.: Surface-based remote sensing of the mixing-layer height – a review, *Meteorol. Z.*, 17, 621–630, 2008.
- Emeis, S., Schäfer, K., Münkel, C., Friedl, R., and Suppan, P.: Evaluation of the interpretation of ceilometer data with RASS and radiosonde data, *Bound.-Lay. Meteorol.*, 143, 25–35, 2012.
- Eresmaa, N., Karppinen, A., Joffre, S. M., Räsänen, J., and Talvitie, H.: Mixing height determination by ceilometer, *Atmos. Chem. Phys.*, 6, 1485–1493, doi:10.5194/acp-6-1485-2006, 2006.
- Flentje, H., Heese, B., Reichardt, J., and Thomas, W.: Aerosol profiling using the ceilometer network of the German Meteorological Service, *Atmos. Meas. Tech. Discuss.*, 3, 3643–3673, doi:10.5194/amtd-3-3643-2010, 2010.
- Garratt, J. R.: *The Atmospheric Boundary Layer*, Cambridge University Press, Cambridge, UK, 1992.
- Haefelin, M., Angelini, F., Morille, Y., Martucci, G., Frey, S., Gobbi, G. P., Lolli, S., O'Dowd, C. D., Sauvage, L., Xueref-Rémy, I., Wastine, B., and Feist, D. G.: Evaluation of mixing-height retrievals from automatic profiling lidars and ceilometers in view of future integrated networks in Europe, *Bound.-Lay. Meteorol.*, 143, 49–75, 2012.
- Hägeli, P., Steyn, D. G., and Strawbridge, K. B.: Spatial and temporal variability of mixed-layer depth and entrainment zone thickness, *Bound.-Lay. Meteorol.*, 97, 47–71, 2000.
- He, Q. and Mao, J.: Observation of urban mixed layer at Beijing using a micro pulse lidar, *Acta Meteorol. Sin.*, 63, 374–384, 2005 (in Chinese).
- He, Q. S., Mao, J. T., Chen, J. Y., and Hu, Y. Y.: Observational and modeling studies of urban atmospheric boundary-layer height and its evolution mechanisms, *Atmos. Environ.*, 40, 1064–1077, doi:10.1016/j.atmosenv.2005.11.016, 2006.
- Holzworth, C. G.: Estimates of mean maximum mixing depths in the contiguous United States, *Mon. Weather Rev.*, 92, 235–242, 1964.
- Holzworth, C. G.: Mixing depths, wind speeds and air pollution potential for selected locations in the United States, *J. Appl. Meteorol.*, 6, 1039–1044, 1967.
- Hu, X., Ma, Z., Lin, W., Zhang, H., Hu, J., Wang, Y., Xu, X., Fuentes, J. D., and Xue, M.: Impact of the Loess Plateau on the atmospheric boundary layer structure and

[Title Page](#)[Abstract](#)[Introduction](#)[Conclusions](#)[References](#)[Tables](#)[Figures](#)[◀](#)[▶](#)[Back](#)[Close](#)[Full Screen / Esc](#)[Printer-friendly Version](#)[Interactive Discussion](#)

air quality in the North China Plain: a case study, *Sci. Total Environ.*, 499, 228–237, doi:10.1016/j.scitotenv.2014.08.053, 2014.

Hyun, Y., Kim, K., and Ha, K.: A comparison of methods to estimate the height of stable boundary layer over a temperate grassland, *Agr. Forest Meteorol.*, 132, 132–142, doi:10.1016/j.agrformet.2005.03.010, 2005.

5 Kamp, D. and McKendry, I.: Diurnal and seasonal trends in convective mixed-layer heights estimated from two years of continuous ceilometer observations in Vancouver, BC, *Bound.-Lay. Meteorol.*, 137, 459–475, 2010.

10 Kunz, G. J., Leeuw, G., Becker, E., and O'Dowd, C. D.: Lidar observations of atmospheric boundary layer structure and sea spray aerosol plumes generation and transport at Mace Head, Ireland (PARFORCE experiment), *J. Geophys. Res.*, 107, 8106, doi:10.1029/2001JD001240, 2002.

15 Li, M., Tang, G., Huang, J., Liu, Z., An, J., and Wang, Y.: Characteristics of winter atmospheric mixing layer height in Beijing-Tianjin-Hebei region and their relationship with the atmospheric pollution, *Environ. Sci.*, 36, 1935–1943, 2015 (in Chinese).

Liu, Z., Hu, B., Wang, L., Wu, F., Gao, W., and Wang, Y.: Seasonal and diurnal variation in particulate matter ( $PM_{10}$  and  $PM_{2.5}$ ) at an urban site of Beijing: analyses from a 9-year study, *Environ. Sci. Pollut. R.*, 22, 627–642, 2015.

20 Luo, T., Yuan, R., and Wang, Z.: Lidar-based remote sensing of atmospheric boundary layer height over land and ocean, *Atmos. Meas. Tech.*, 7, 173–182, doi:10.5194/amt-7-173-2014, 2014.

McKendry, I. G., Kamp, D., Strawbridge, K. B., Christen, A., and Crawford, B.: Simultaneous observations of boundary-layer aerosol layers with CL31 ceilometer and 1064/532 nm lidar, *Atmos. Environ.*, 43, 5847–5852, doi:10.1016/j.atmosenv.2009.07.063, 2009.

25 Münkel, C. and Räsänen, J.: New optical concept for commercial lidar ceilometers scanning the boundary layer, *P. SPIE*, 5571, 364–374, 2004.

Münkel, C., Eresmaa, N., Räsänen, J., and Karppinen, A.: Retrieval of mixing height and dust concentration with lidar ceilometer, *Bound.-Lay. Meteorol.*, 124, 117–128, 2007.

30 Muñoz, R. C. and Undurraga, A. A.: Daytime mixed layer over the Santiago Basin: Description of two years of observations with a lidar ceilometer, *J. Appl. Meteorol. Clim.*, 49, 1728–1741, 2010.

[Title Page](#)

[Abstract](#)

[Introduction](#)

[Conclusions](#)

[References](#)

[Tables](#)

[Figures](#)

◀

▶

◀

▶

[Back](#)

[Close](#)

[Full Screen / Esc](#)

[Printer-friendly Version](#)

[Interactive Discussion](#)



## Mixing layer height and air pollution over Beijing

G. Tang et al.

[Title Page](#)

[Abstract](#)

[Introduction](#)

[Conclusions](#)

[References](#)

[Tables](#)

[Figures](#)

◀

▶

◀

▶

[Back](#)

[Close](#)

[Full Screen / Esc](#)

[Printer-friendly Version](#)

[Interactive Discussion](#)



<a href="#">Title Page</a>	
<a href="#">Abstract</a>	<a href="#">Introduction</a>
<a href="#">Conclusions</a>	<a href="#">References</a>
<a href="#">Tables</a>	<a href="#">Figures</a>
<a href="#">◀</a>	<a href="#">▶</a>
<a href="#">◀</a>	<a href="#">▶</a>
<a href="#">Back</a>	<a href="#">Close</a>
<a href="#">Full Screen / Esc</a>	
<a href="#">Printer-friendly Version</a>	
<a href="#">Interactive Discussion</a>	



- Stull, R. B.: An Introduction to Boundary Layer Meteorology, Kluwer Academic Publishers, Dordrecht, 1988.
- Tang, G., Li, X., Wang, Y., Xin, J., and Ren, X.: Surface ozone trend details and interpretations in Beijing, 2001–2006, *Atmos. Chem. Phys.*, 9, 8813–8823, doi:10.5194/acp-9-8813-2009, 2009.
- Tang, G., Wang, Y., Li, X., Ji, D., Hsu, S., and Gao, X.: Spatial-temporal variations in surface ozone in Northern China as observed during 2009–2010 and possible implications for future air quality control strategies, *Atmos. Chem. Phys.*, 12, 2757–2776, doi:10.5194/acp-12-2757-2012, 2012.
- Tang, G., Zhu, X., Hu, B., Xin, J., Wang, L., Münkel, C., Mao, G., and Wang, Y.: Vertical variations of aerosols and the effects responded to the emission control: application of lidar ceilometer in Beijing during APEC, 2014, *Atmos. Chem. Phys. Discuss.*, 15, 13173–13209, doi:10.5194/acpd-15-13173-2015, 2015.
- Vogelezang, D. H. P. and Holtslag, A. A. M.: Evolution and model impacts of alternative boundary layer formulations, *Bound.-Lay. Meteorol.*, 81, 245–269, 1996.
- Wang, X. Y. and Wang, K. C.: Estimation of atmospheric mixing layer height from radiosonde data, *Atmos. Meas. Tech.*, 7, 1701–1709, doi:10.5194/amt-7-1701-2014, 2014.
- Wang, Z., Cao, X., Zhang, L., Notholt, J., Zhou, B., Liu, R., and Zhang, B.: Lidar measurement of planetary boundary layer height and comparison with microwave profiling radiometer observation, *Atmos. Meas. Tech.*, 5, 1965–1972, doi:10.5194/amt-5-1965-2012, 2012.
- White, A. B., Senff, C. J., and Banta, R. M.: A Comparison of mixing depths observed by ground-based wind profilers and an airborne lidar, *J. Atmos. Ocean. Tech.*, 16, 584–590, 1999.
- Wiegner, M., Emeis, S., Freudenthaler, V., Heese, B., Junkermann, W., Münkel, C., Schäfer, K., Seefeldner, M., and Vogt, S.: Mixing layer height over Munich, Germany: variability and comparisons of different methodologies, *J. Geophys. Res.*, 111, D13201, doi:10.1029/2005JD006593, 2006.
- Xin, J., Wang, Y., Tang, G., Wang, L., Sun, Y., Wang, Y. H., Hu, B., Song, T., Ji, D. S., Wang, W. F., Li, L., and Liu, G. R.: Variability and reduction of atmospheric pollutants in Beijing and its surrounding area during the Beijing 2008 Olympic Games, *Chinese Sci. Bull.*, 55, 1937–1944, 2010.
- Yang, D. W., Li, C., Lau, A. K.-H., and Li, Y.: Long-term measurement of daytime atmospheric mixing layer height over Hong Kong, *J. Geophys. Res.*, 118, 2422–2433, 2013.

Mixing layer height  
and air pollution over  
Beijing

G. Tang et al.

- Yang, H., Liu, W., Lu, Y., Xie, P., Xu, L., Zhao, X., Yu, T., and Yu, J.: PBL observations by lidar at Peking, Optical Tech., 31, 221–226, 2005.
- Ye, X., Wu, B., and Zhang, H.: The turbulent structure and transport in fog layers observed over the Tianjin area, Atmos. Res., 153, 217–234, doi:10.1016/j.atmosres.2014.08.003, 2015.
- Zhang, J. K., Sun, Y., Liu, Z. R., Ji, D. S., Hu, B., Liu, Q., and Wang, Y. S.: Characterization of submicron aerosols during a month of serious pollution in Beijing, 2013, Atmos. Chem. Phys., 14, 2887–2903, doi:10.5194/acp-14-2887-2014, 2014.
- Zhang, Q., Quan, J., Tie, X., Li, X., Liu, Q., Gao, Y., and Zhao, D.: Effects of meteorology and secondary particle formation on visibility during heavy haze events in Beijing, China, Sci. Total Environ., 502, 578–584, doi:10.1016/j.scitotenv.2014.09.079, 2015.
- Zhang, X., Cai, X., and Chai, F.: Structures and characteristics of the atmospheric boundary layer over Beijing area in autumn, Acta Sci. Natur. Univ. Pekinensis, 42, 220–225, 2006 (in Chinese).
- Zilitinkevich, S. and Baklanov, A.: Calculation of the height of the stable boundary layer in practical applications, Bound.-Lay. Meteorol., 105, 389–409, 2002.

<a href="#">Title Page</a>	
<a href="#">Abstract</a>	<a href="#">Introduction</a>
<a href="#">Conclusions</a>	<a href="#">References</a>
<a href="#">Tables</a>	<a href="#">Figures</a>
<a href="#">◀</a>	<a href="#">▶</a>
<a href="#">◀</a>	<a href="#">▶</a>
<a href="#">Back</a>	<a href="#">Close</a>
<a href="#">Full Screen / Esc</a>	
<a href="#">Printer-friendly Version</a>	
<a href="#">Interactive Discussion</a>	



## Mixing layer height and air pollution over Beijing

G. Tang et al.

**Table 1.** Site description and instrument list. BJT refers to the Beijing tower; ZBAA is the international standard weather station.

Sites	Long, lat	Instruments	Time interval	Time resolution
BJT	116.37, 39.97	CL31	15 Jul 2009–31 Dec 2012	10 min
		PM <sub>2.5</sub> , PM <sub>10</sub>	15 Jul 2009–31 Dec 2012	60 min
		Tower-based meteorology	15 Jul 2009–31 Dec 2012	5 min
ZBAA	116.28, 39.48	Weather balloons	15 Jul 2009–31 Dec 2012	1 per week at 14:00 LT
		Weather balloons	1 Jan 2012–31 Dec 2012	08:00 and 20:00 LT
		Ground-based meteorology	15 Jul 2009–31 Dec 2012	30 min

**Mixing layer height  
and air pollution over  
Beijing**

G. Tang et al.

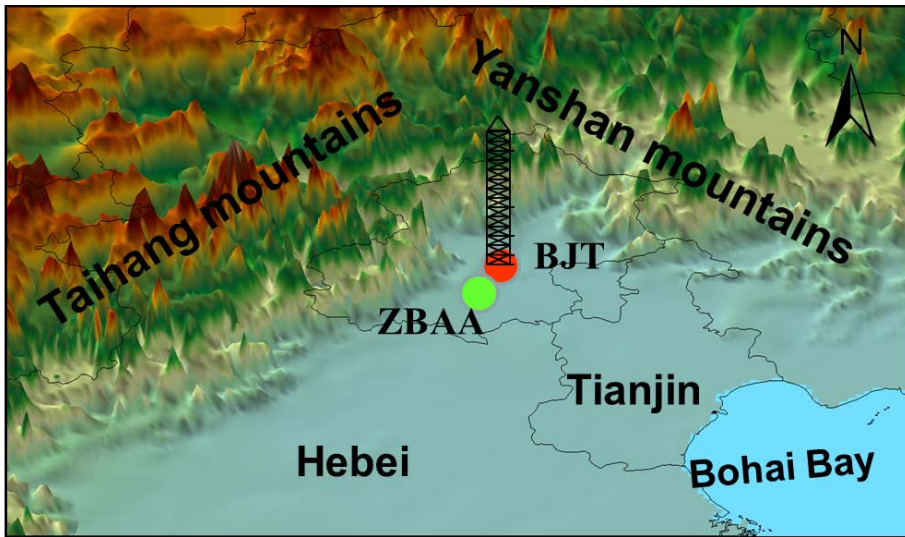


**Figure 1.** Topography and the observation sites.

[Title Page](#)[Abstract](#)[Introduction](#)[Conclusions](#)[References](#)[Tables](#)[Figures](#)[|◀](#)[▶|](#)[◀](#)[▶](#)[Back](#)[Close](#)[Full Screen / Esc](#)[Printer-friendly Version](#)[Interactive Discussion](#)

**Mixing layer height  
and air pollution over  
Beijing**

G. Tang et al.

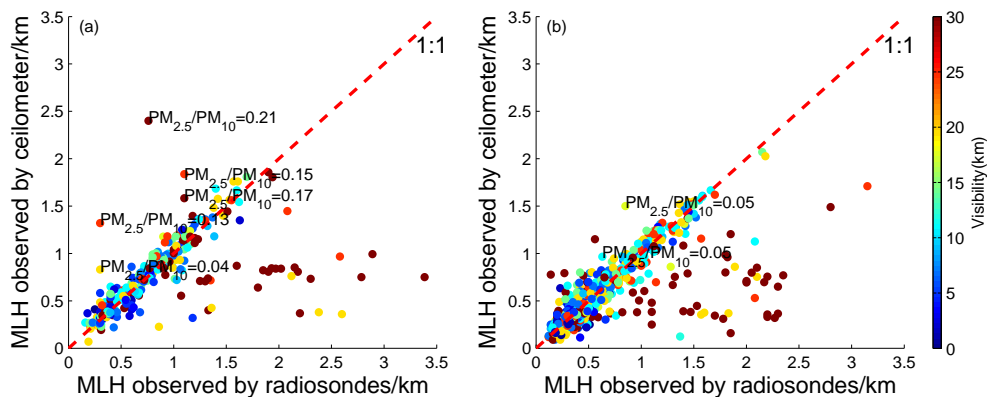


**Figure 2.** The comparison of MLH between radiosondes and the ceilometer according to visibility for convective **(a)** and stable **(b)** states.

**Mixing layer height  
and air pollution over  
Beijing**

G. Tang et al.

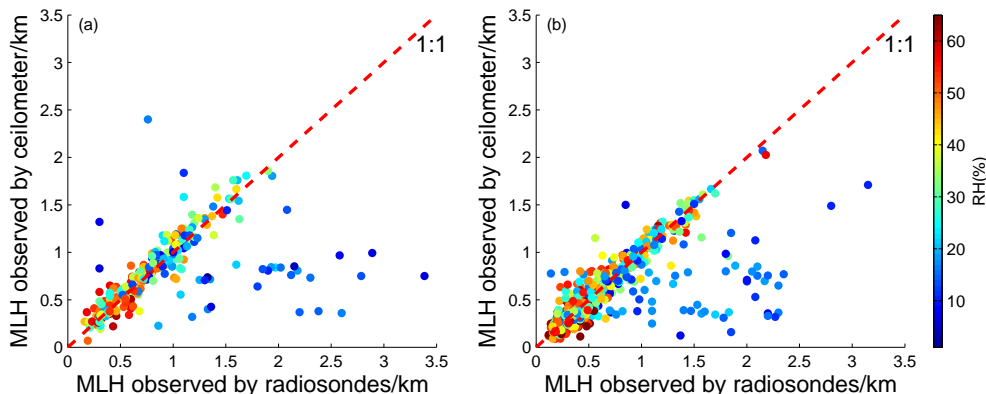


**Figure 3.** The comparison of MLH between radiosondes and the ceilometer according to humidity for convective **(a)** and stable **(b)** states.

**Mixing layer height  
and air pollution over  
Beijing**

G. Tang et al.

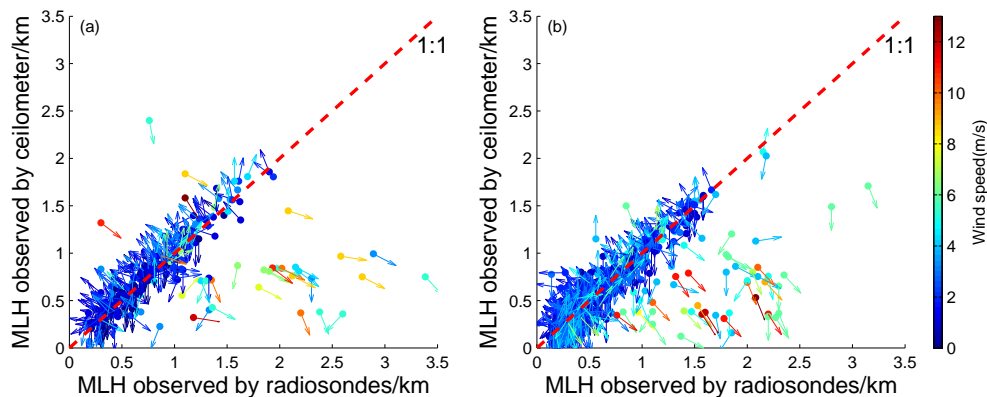


**Figure 4.** The comparison of MLH between radiosondes and the ceilometer according to vector winds for convective **(a)** and stable **(b)** states.

- [Title Page](#)
- [Abstract](#) [Introduction](#)
- [Conclusions](#) [References](#)
- [Tables](#) [Figures](#)
- [◀](#) [▶](#)
- [◀](#) [▶](#)
- [Back](#) [Close](#)
- [Full Screen / Esc](#)
- [Printer-friendly Version](#)
- [Interactive Discussion](#)



**Mixing layer height and air pollution over Beijing**

G. Tang et al.

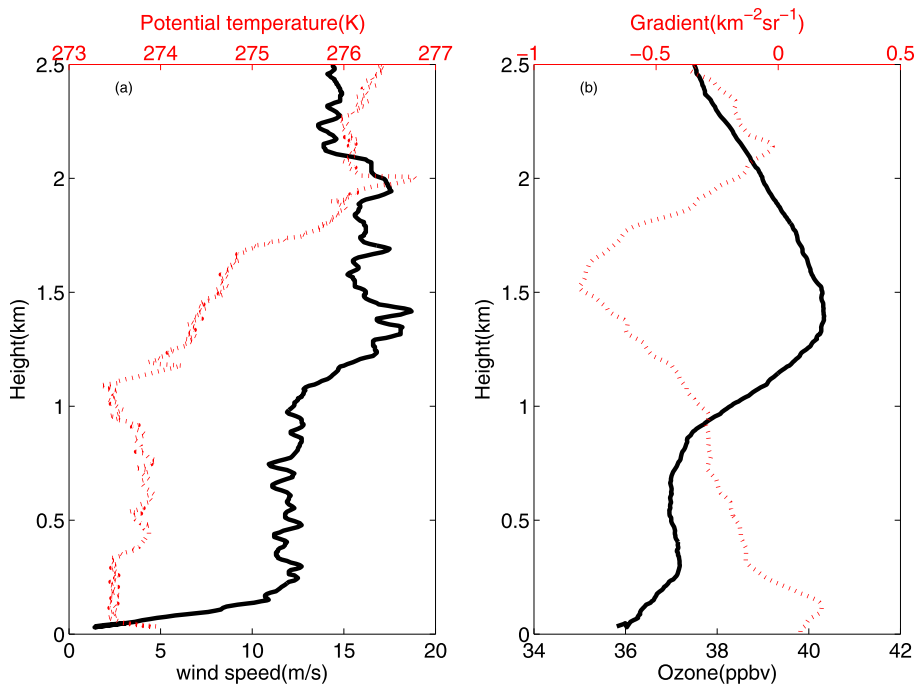


**Figure 5.** The virtual potential temperature and wind speed **(a)**, and ozone and backscatter gradients **(b)** at 14:00 LT on 29 December 2009 in Beijing.

**Mixing layer height  
and air pollution over  
Beijing**

G. Tang et al.

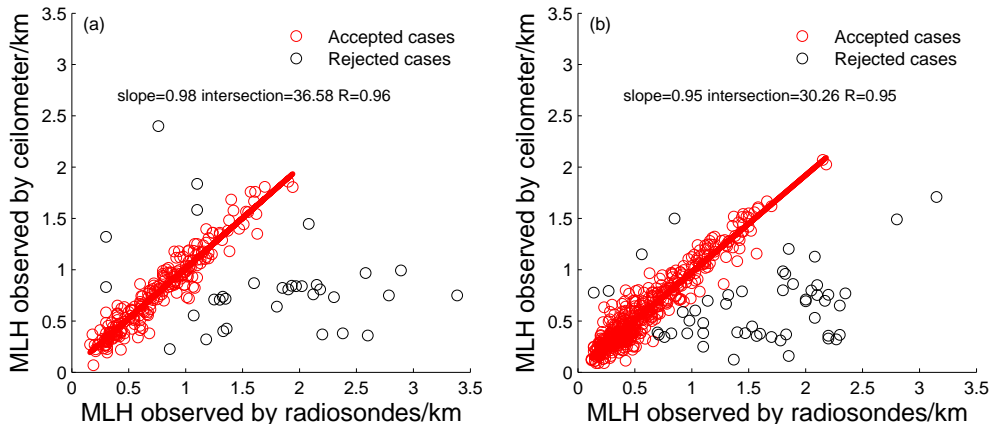


**Figure 6.** The comparison of MLH between the ceilometer and radiosondes for convective (a) and stable (b) states.

## Discussion Paper | Mixing layer height and air pollution over Beijing

G. Tang et al.

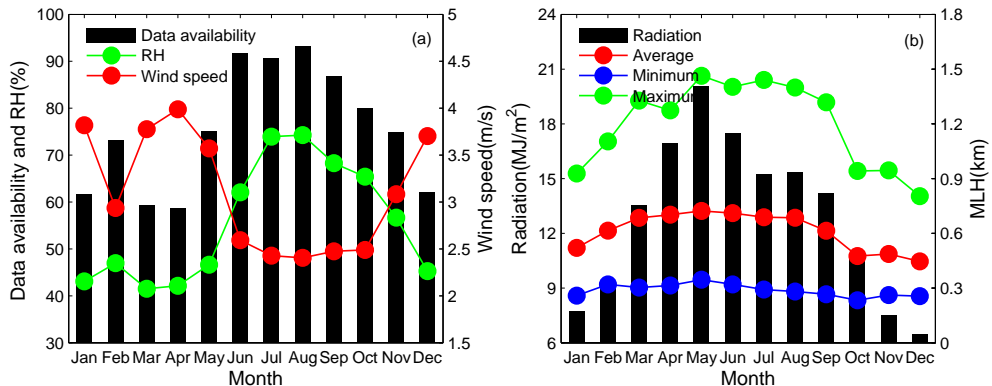


**Figure 7.** Monthly variations in the effective rate, wind speed, and relative humidity (RH) (a), and MLH and total radiation flux (b) in Beijing.

- [Title Page](#)
- [Abstract](#) [Introduction](#)
- [Conclusions](#) [References](#)
- [Tables](#) [Figures](#)
- [◀](#) [▶](#)
- [Back](#) [Close](#)
- [Full Screen / Esc](#)
- [Printer-friendly Version](#)
- [Interactive Discussion](#)



**Mixing layer height  
and air pollution over  
Beijing**

G. Tang et al.

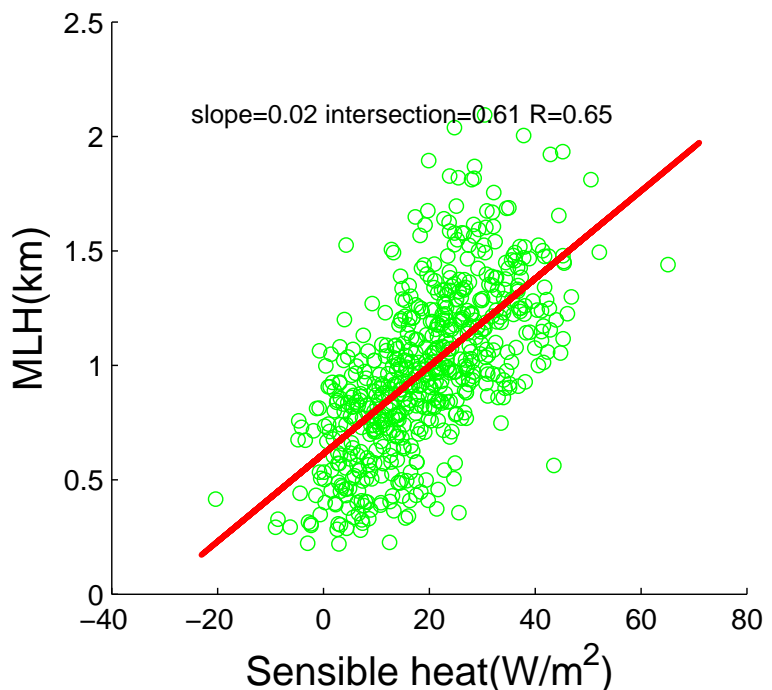


**Figure 8.** The correlation between the sensible heat and MLH in Beijing.

**Mixing layer height  
and air pollution over  
Beijing**

G. Tang et al.

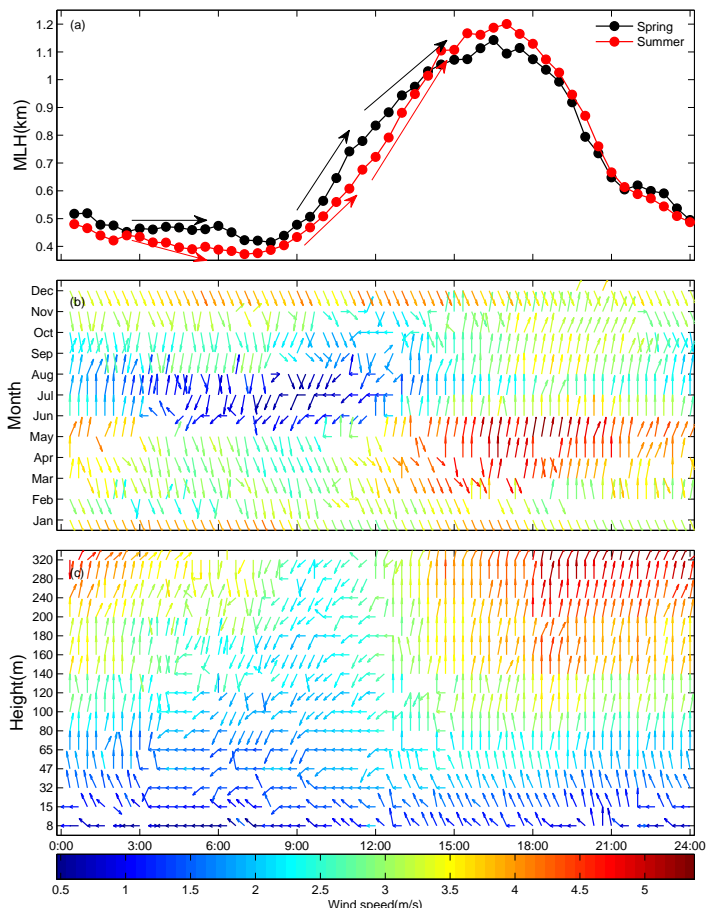


**Figure 9.** The daily variations in MLH in spring and summer (a), seasonal wind vectors at 100 m (b), and vertical profiles of wind vectors in July (c) in Beijing.

## Mixing layer height and air pollution over Beijing

G. Tang et al.

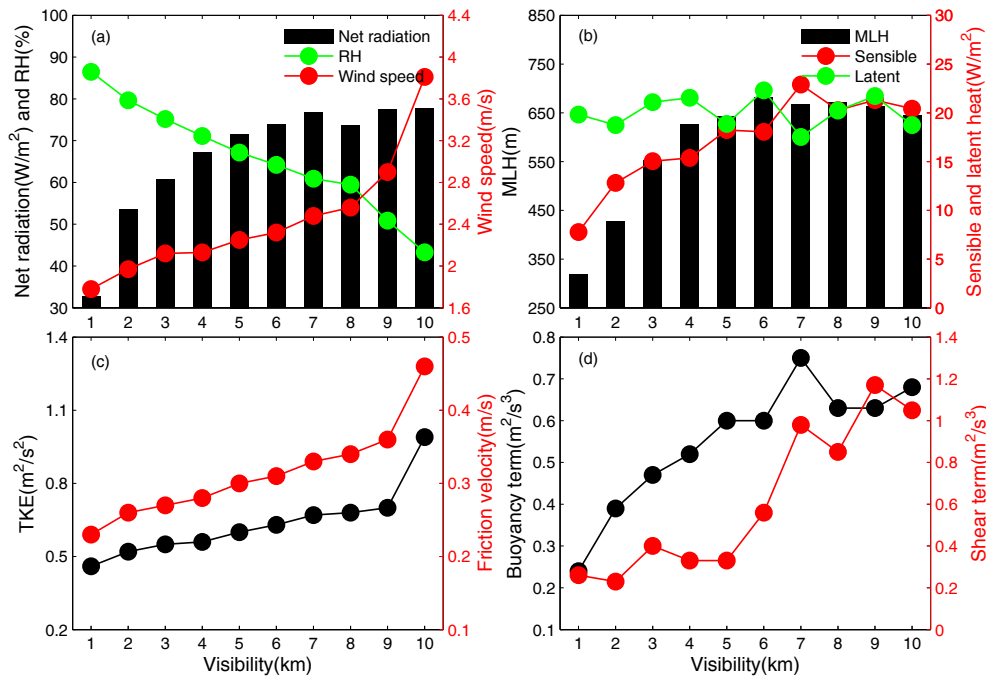


**Figure 10.** The variations in net radiation, relative humidity (RH), and wind speed **(a)**, MLH, sensible and latent heat **(b)**, TKE, and fraction velocity **(c)**, and buoyancy and shear term in TKE **(d)** according to different visibility levels.

**Mixing layer height  
and air pollution over  
Beijing**

G. Tang et al.

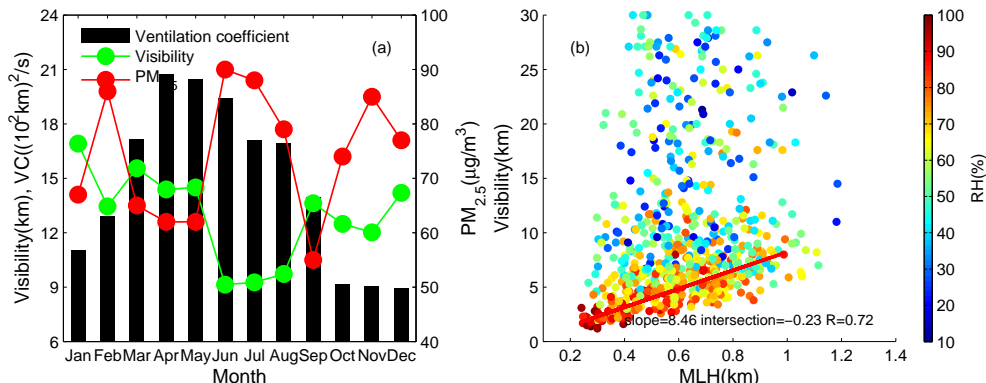


**Figure 11.** Monthly variations in visibility and ventilation coefficients (a) and the correlation between the MLH and visibility according to the relative humidity (RH) (b) in Beijing.